ISSN: 2710-0588

Study on the Micro-Mechanism of Surfactant-Driven Oil Recovery and the Evolution of Residual Oil Distribution based on Microfluidics

Jiaxuan Ma, Wei Xiao, and Yuanyuan Peng

School of Xi'an Shiyou University, Xi'an 710065, China

Abstract

Due to their minute throats and strong heterogeneity, tight reservoirs are prone to forming bypass channels during conventional water flooding, resulting in low recovery rates. To elucidate the microscopic oil displacement mechanism of surfactants, this study constructed a heterogeneous microfluidic model featuring typical throat characteristics. Visualization experiments were conducted to compare the performance of water flooding versus surfactant flooding. Results indicate: - Water flooding leaves residual oil predominantly in networked and columnar patterns, achieving a final recovery rate of approximately 43%; Surfactants, by reducing oil-water interfacial tension and modulating wettability, weakened capillary confinement. This transformed residual oil into columnar and isolated droplet forms, boosting recovery to approximately 65%. The treatment significantly enhanced mobilization of large and medium-pore residual oil but remained ineffective for small-pore network residual oil. This study provides experimental and theoretical support for optimizing chemical flooding in tight reservoirs.

Keywords

Tight Reservoirs, Surfactant Flooding, Microfluidics, Residual Oil, Recovery Rate.

1. Introduction

Tight reservoirs, constrained by inherent characteristics such as minute pore-throat dimensions, high heterogeneity, and significant flow resistance, readily form water bypass channels during conventional waterflood development[1]. This leads to highly dispersed residual oil distribution and generally low overall recovery rates. Extensive research indicates that at the micrometer-scale pore throat dimension, capillary forces, oil-water interfacial tension, and wettability critically govern fluid migration behavior. Particularly in low-permeability to ultra-low-permeability tight reservoirs, interfacial effects often significantly outweigh viscous and gravitational forces. Consequently, effectively mitigating capillary confinement and enhancing displacement efficiency emerge as central scientific challenges in enhancing recovery rates for tight reservoirs[2].

Based on extensive validation from secondary development practices in mature oilfields, surfactants significantly enhance the mobility of trapped oil droplets through multiple mechanisms. These include reducing oil-water interfacial tension, regulating rock surface wettability, and inducing emulsification and interfacial disturbance. Consequently, surfactants represent a crucial technological approach for chemically enhanced oil recovery in tight reservoirs[3]. However, constrained by the spatial resolution and visualization limitations of traditional core displacement experiments, direct and clear experimental evidence supporting the action mechanisms of surfactants in micro-scale pore throats and their oil displacement mechanisms remains lacking[4].

ISSN: 2710-0588

In recent years, microfluidic technology has emerged as a crucial experimental tool for investigating the microscopic mechanisms of multiphase flow. This advancement stems from its distinct advantages in precisely constructing pore structures, accurately controlling fluid properties and displacement conditions, and enabling real-time visualization of dynamic oil-water interface processes. Related studies have achieved a series of advances in residual oil formation mechanisms, droplet deformation and breakup, wettability control, and capillary entrapment behavior, providing a new technical platform for investigating chemical drive mechanisms in tight reservoirs[5]. Compared to idealized homogeneous models, heterogeneous microfluidic models constructed based on the actual throat characteristics of tight reservoirs are more conducive to revealing the actual displacement behavior of surfactants within complex pore networks.

Currently, research on surfactant microfluidic oil displacement primarily focuses on qualitative characterization of overall displacement efficiency, while insufficient attention is paid to the specific forms of residual oil (e.g., isolated oil droplets, columnar oil, and networked oil) within different pore structures (such as macropores, mesopores, and micropores). Given this, it is necessary to conduct high-resolution visual microfluidic surfactant displacement experiments that incorporate typical throat structures of tight reservoirs, enabling a more systematic and in-depth analysis of the microscopic oil displacement process[6].

Based on the above understanding, this paper constructed a heterogeneous microfluidic model representing the pore-throat characteristics of tight oil reservoirs and systematically conducted visual experiments on surfactant displacement of crude oil. Through dynamic observation of oil-water interface evolution during displacement and quantitative identification and statistical analysis of residual oil forms in different pore structures, this study elucidates the microscopic oil displacement mechanism of surfactants in tight reservoirs. It provides reliable experimental techniques and theoretical support for optimizing chemical flooding parameters and field applications[7].

2. Surfactant Water-Flooding Microfluidic Experiment

Surfactant water-flooding microfluidic experiments serve as a high-resolution visualization technique for elucidating the microscopic oil displacement mechanisms in tight reservoirs. This method involves constructing microfluidic chips mimicking the characteristic pore-throat structures of typical tight reservoirs. Under precisely controlled flow conditions and displacement regimes, surfactant solutions are introduced to displace crude oil within the pores. Leveraging high-resolution microscopic imaging and image acquisition systems, it enables real-time capture of oil-water interface evolution, clearly observing microscopic dynamic behaviors such as oil droplet deformation, breakup, coalescence, detachment, and redistribution. This facilitates quantitative analysis of transformation and evolution patterns for different residual oil phases. This experimental approach provides direct insights into the mechanism by which surfactants weaken capillary confinement and enhance oil phase mobility, offering reliable microscopic support and experimental evidence for surfactant flooding to improve recovery rates in tight reservoirs

2.1. Surfactant Water-Flooding Microfluidic Experimental Setup

The experimental apparatus comprises five functionally integrated components: a heterogeneous porous medium microfluidic chip, a displacement apparatus, a microscopic imaging system, an air compressor, and a monitor. Together, these elements form a comprehensive testing platform for surfactant water-flooding microfluidic experiments.

(1) Microfluidic chip for heterogeneous porous media: Designed to simulate the complex pore-throat structure characteristics found in tight reservoirs. The internal geometry of the chip is

ISSN: 2710-0588

constructed based on the actual pore-throat size distribution and connectivity relationships within real reservoirs, incorporating multi-scale pore units such as large, medium, and small pores to accurately depict the significant spatial heterogeneity of tight reservoirs. The chip material typically employs glass or glass-like media with excellent optical transparency, enabling clear visualization of oil-water two-phase flow and interfacial evolution during experiments. Simultaneously, surface modification of the chip's inner walls effectively simulates different wettability conditions, providing a reliable physical foundation for studying the reservoir state and migration characteristics of residual oil during surfactant displacement processes.

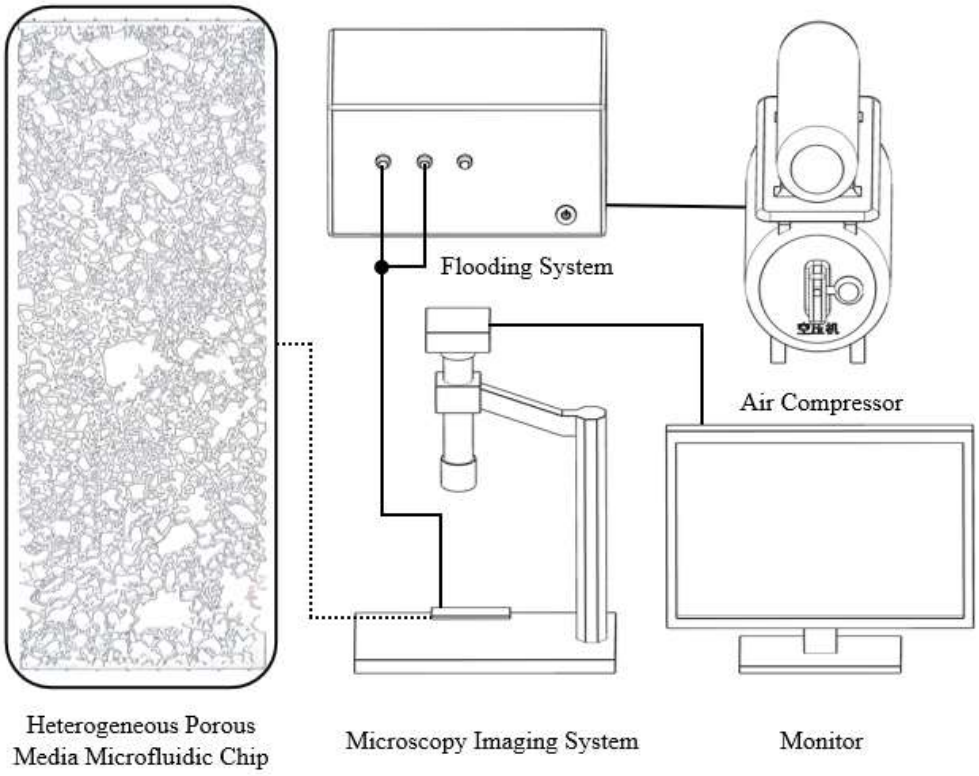

Fig. 1 Schematic Diagram of the Experimental Setup

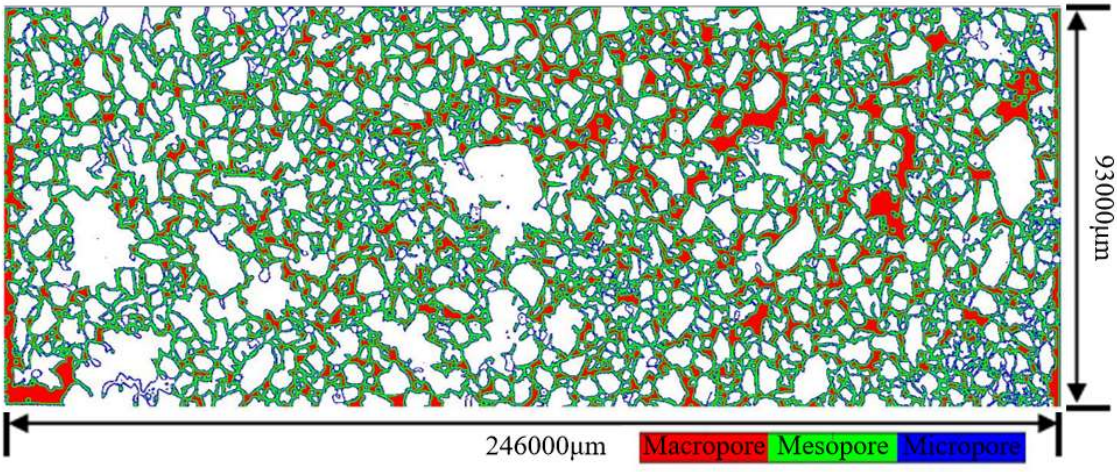

Fig. 2 Schematic diagram of pore distribution structure in microfluidic chip

ISSN: 2710-0588

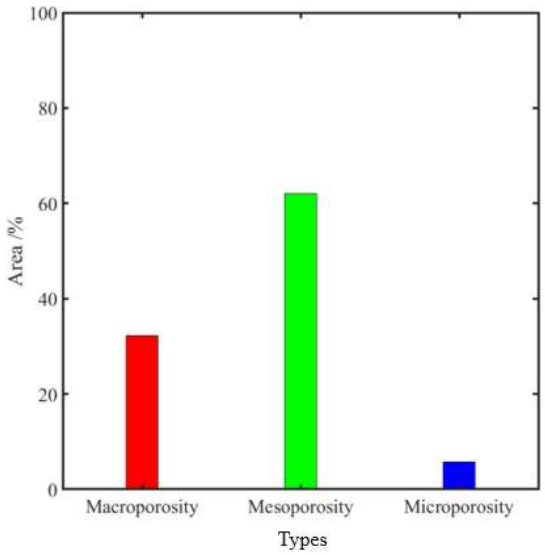

Fig. 3 Distribution of pore types in the microfluidic chip

For quantitative characterization of pore structure, the Maximum Inscribed Sphere (MIS) algorithm is applied to perform Euclidean distance transformation on the binarized pore regions. Local maxima in the distance field correspond to the maximum equivalent sphere radius accommodated within the pore, with twice this value defined as the local pore scale. Furthermore, a quantile method is employed to statistically partition the pore size distribution into three categories: large pores, medium pores, and small pores. This approach provides an intuitive visualization of the multiscale characteristics inherent in the pore structure of dense porous media.

(2) Displacement System: Primarily used to achieve stable and precise injection of experimental fluids, this system is the key equipment ensuring controllability of the displacement process. This system enables precise control over injection flow rate, displacement rate, and injection sequence. Typically employing high-precision syringe pumps or constant-flow displacement devices, it sequentially injects simulated formation water, surfactant solutions, and crude oil into the microfluidic chip according to a preset protocol. This establishes repeatable displacement conditions with comparable results, ensuring the stability, reliability, and reproducibility of experimental data.

(3) Micro-imaging System: Comprising an optical microscope, high-resolution camera, and integrated light source, this system is primarily used for real-time acquisition of oil-water two-phase flow states and interfacial changes within microfluidic chips. It continuously records the deformation, breakup, migration, and coalescence of oil droplets, along with the evolution of residual oil morphologies of various types, providing high-quality raw data support for subsequent image-processing-based quantitative analysis.

(4) Air Compressor: Provides a stable air supply for the entire displacement system, primarily used for pressure compensation in displacement instruments or auxiliary fluid delivery to ensure continuous and stable injection pressure during experiments. Its output pressure can be flexibly adjusted according to different experimental conditions, thereby meeting experimental requirements under varying displacement rates and pressure conditions.

(5) Monitor: Used to display in real time the images and video information captured by the microscopic imaging system, enabling experimenters to visually and continuously monitor the displacement process and the evolution of the oil-water interface. Simultaneously, the monitor facilitates immediate parameter adjustments and anomaly detection during experiments, thereby enhancing operational safety, stability, and overall efficiency.

ISSN: 2710-0588

Sub heading

When receiving the paper, we assume that the corresponding authors grant us the copyright to use the paper for the book or journal in question. When receiving the paper, we assume that the corresponding authors grant us the copyright to use the paper for the book or journal in question. When receiving the paper, we assume that the corresponding authors grant us the copyright to use.

2.2. Experimental Fluid.

The simulated formation water used in the experiment was prepared by mixing deionized water with analytical-grade reagents (NaCl, $CaCl_2$, $MgCl_2 \cdot 6H_2O$, etc.) to achieve the ionic concentrations shown in Table 1. The pH was adjusted to 7.5 ± 0.2. Viscosity was measured at 25°C using a Ubbelohde viscometer (model: capillary inner diameter 0.5 mm), yielding a value of 1.02 mPa·s. Density was determined via the hydrometer method as 1.03 g/cm^3.

Table 1. Ionic composition of simulated formation water

Ionic composition(mg·L^{-1})						Total salinity(mg·L^{-1})
Cl^-	SO_4^{2-}	HCO_3^-	Na^+	Ca^{2+}	Mg^{2+}	
1.54×10^5	5×10^3	0.42×10^3	7×10^4	1.48×10^4	2.03×10^3	2.5×10^5

The experimental oil used was oil-soluble red-stained simulated oil, with a viscosity of 10.0 mPa·s and a density of 0.89 g/cm^3 at 20°C. The oil-water interfacial tension was measured at 25°C using the hanging drop method (instrument model: Krüss DSA100) and found to be 28.5 mN/m. Prior to testing, crude oil and simulated formation water were equilibrated for 24 hours in a 25°C constant-temperature chamber to ensure stable fluid properties and enhance the reproducibility and comparability of experimental results.

2.3. Experimental Procedure

The specific steps for the surfactant water-flooding microfluidic experiment are as follows:

(1) Cleaning and pretreatment of microfluidic chips for heterogeneous porous media. The chip channels are sequentially flushed with anhydrous ethanol and deionized water to remove impurities and bubbles, followed by degassing under vacuum conditions to prevent gas entrapment from interfering with flow during experiments. Subsequently, surface wettability is engineered according to experimental requirements to achieve stable hydrophilic or mildly lipophilic states.

(2) Slowly inject simulated water into the microfluidic chip to fully saturate the channels, confirming no residual bubbles remain within the pores via the microscopic imaging system. Subsequently, switch the injected fluid to simulated oil and drive out the simulated water at a constant flow rate until the aqueous phase within the chip is largely replaced by crude oil, establishing the initial oil-saturated state. Document the distribution characteristics of the oil phase within the pores.

(3) Conduct a benchmark waterflooding experiment. Re-inject simulated water into the chip and perform waterflooding under constant flow conditions until the outlet oil content decreases significantly and stabilizes, forming a stable residual oil distribution state. Continuously acquire images through the microscopic imaging system to analyze the occurrence patterns and spatial distribution of residual oil under waterflooding conditions.

(4) Following completion of the benchmark water flooding, the injection fluid was switched to a prepared surfactant solution, and surfactant flooding experiments were conducted under identical flow conditions. The evolution of the oil-water interface, oil droplet deformation, and

ISSN: 2710-0588

migration behavior during displacement were recorded in real time, with particular focus on the initiation and stripping processes of residual oil within different pore throat structures.

(5) Once the displacement process reached a steady state, injection was halted, and the experimental data were organized and analyzed. Quantitative statistics on residual oil saturation, oil droplet size distribution, and interfacial morphology changes were obtained through image processing methods. These results were compared with the baseline water-flooding outcomes to elucidate the mechanism by which surfactants enhance micro-scale oil displacement efficiency.

2.4. Data Processing

The processing of microfluidic experimental data is primarily accomplished using ImageJ and MATLAB software, following this workflow:

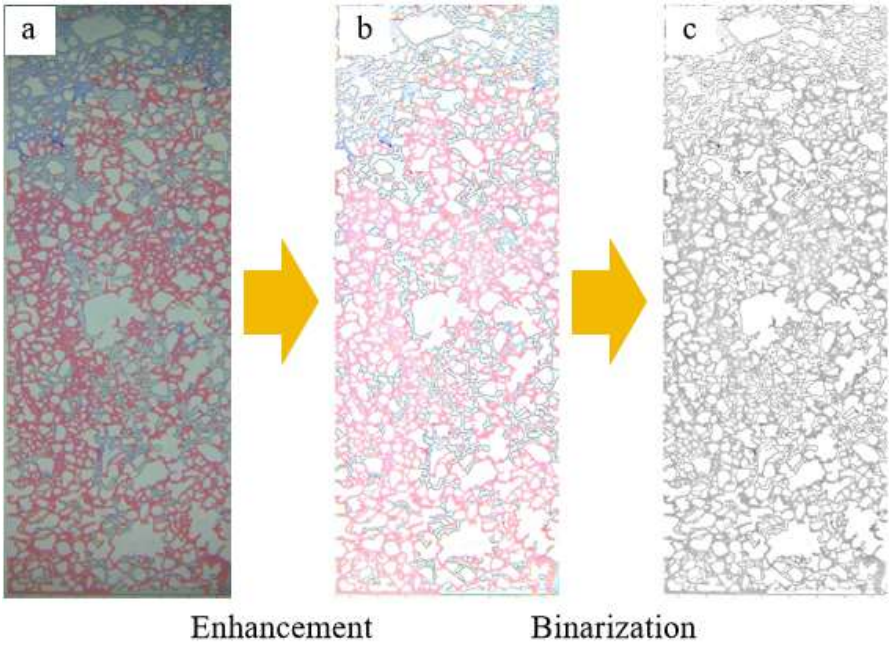

Fig. 4 Image Processing Workflow

Experimental videos or sequential images captured by the microscopic imaging system are imported into ImageJ for preprocessing. Raw color images undergo uniform enhancement processing, followed by brightness and contrast adjustments, background subtraction, and median filtering to amplify grayscale differences between oil and water phases, thereby improving interface recognition clarity. The processed images are then segmented through binarization in ImageJ. By setting appropriate thresholds, the oil and water phases were effectively distinguished. Morphological operations (filling holes, removing isolated noise points) were applied to the binary images to obtain continuous, accurate oil distribution maps. Based on the binary results, the oil area within a single frame could be directly calculated. Fundamental data such as oil area, residual oil saturation, and oil droplet size at each time point were exported and saved in TXT format. Import the data exported from ImageJ into MATLAB for further processing and analysis. In MATLAB, organize the data into time series and perform normalization. Calculate parameters such as the residual oil change rate and the improvement in oil recovery efficiency across different displacement stages. Based on connected component analysis, statistically analyze the oil droplet size distribution, quantity changes, and evolution patterns. Plot the oil phase area curve over time.

ISSN: 2710-0588

2.5. Residual Oil Identification

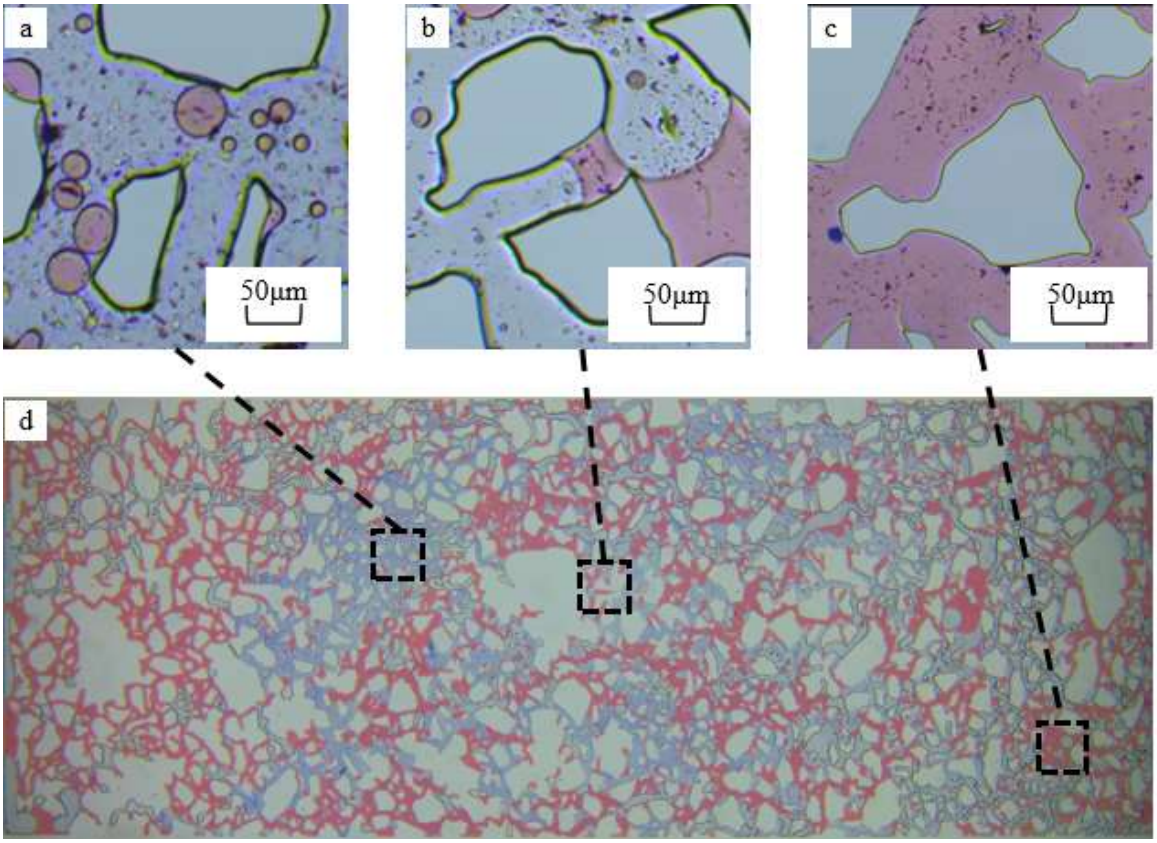

Fig. 5 Residual Oil Identification

3. Experimental results

3.1. Water-Driven Microfluidic Experiment Results

3.1.1. Water-Driven Microfluidic Experiment: Displacement Effect and Interface Evolution Process

The experimental results above reflect the evolution characteristics of residual oil at the microscopic level and the variation patterns of recovery rate during water flooding. Figures (a–f) show that as water flooding progresses, the oil phase (red) within pores is gradually displaced, though overall displacement efficiency remains limited. During the initial phase (0–20 s), the water phase rapidly advances along dominant pathways, preferentially displacing connected oil and reducing the oil phase area. Correspondingly, the recovery rate rises sharply from 0 to approximately 21%. However, due to high interfacial tension and dominant capillary forces, substantial oil remains trapped within pore throat structures as continuous films or corner oil. During the intermediate stage (20–60 s), water drive primarily advances along existing flow pathways, mobilizing limited additional oil. The distribution pattern of residual oil shows little change, with recovery rate only gradually increasing from approximately 21% to about 27%. By approximately 80 seconds, the recovery rate reached about 40%. However, microscopic images revealed that residual oil primarily persisted as interconnected oil bands and localized oil aggregates, without undergoing significant fragmentation or dispersion. During the late waterflooding phase (80–140 s), dominant flow pathways gradually stabilized, with pronounced water flow bypassing. The water phase exhibited limited mobilization capacity for isolated oil and corner oil constrained by capillary forces, leading to a stable oil distribution pattern (Figure g). Recovery rate growth significantly slowed during this stage, increasing only marginally from approximately 40% to around 43% before reaching a steady

ISSN: 2710-0588

state. Under waterflooding conditions without surfactant addition, the oil displacement process is primarily governed by dominant channels. While the water phase exhibits some displacement effect on interconnected residual oil, its ability to mobilize membrane oil and isolated oil is limited. This results in the recovery rate rapidly plateauing during the mid-to-late stages, providing a necessary comparative baseline for subsequent introduction of surfactants or other enhanced displacement techniques.

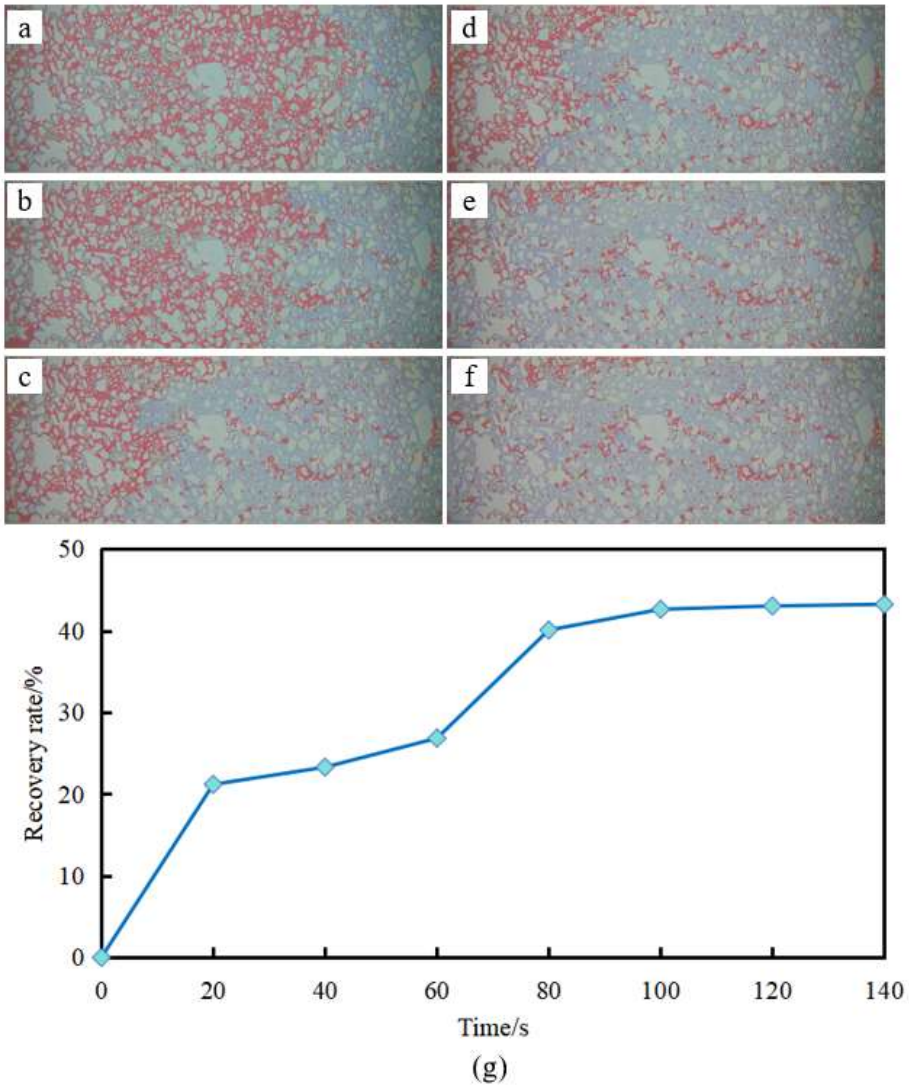

Fig. 6 Microfluidic Water Displacement Results

3.1.2. Microscopic Effects in Water-Driven Microfluidic Experiments

As shown in Fig 7(a–c), under conventional waterflooding conditions, residual oil at the micro-scale exhibits a pronounced heterogeneous distribution pattern. Figure a reveals complex pore structures with uneven connectivity, providing diverse spaces for residual oil accumulation. Figure b shows the identification results of residual oil morphology, indicating that residual oil primarily exists as reticular and columnar forms, with relatively fewer isolated droplets. Network-type residual oil often forms continuous or semi-continuous oil phase networks along pore throat systems, indicating that during water flooding, the water phase tends to break through preferentially along high-permeability pathways, leading to partial oil phase bypass and retention. Columnar residual oil, on the other hand, is primarily distributed within elongated pores and throats, governed by both pore geometry and capillary forces.

ISSN: 2710-0588

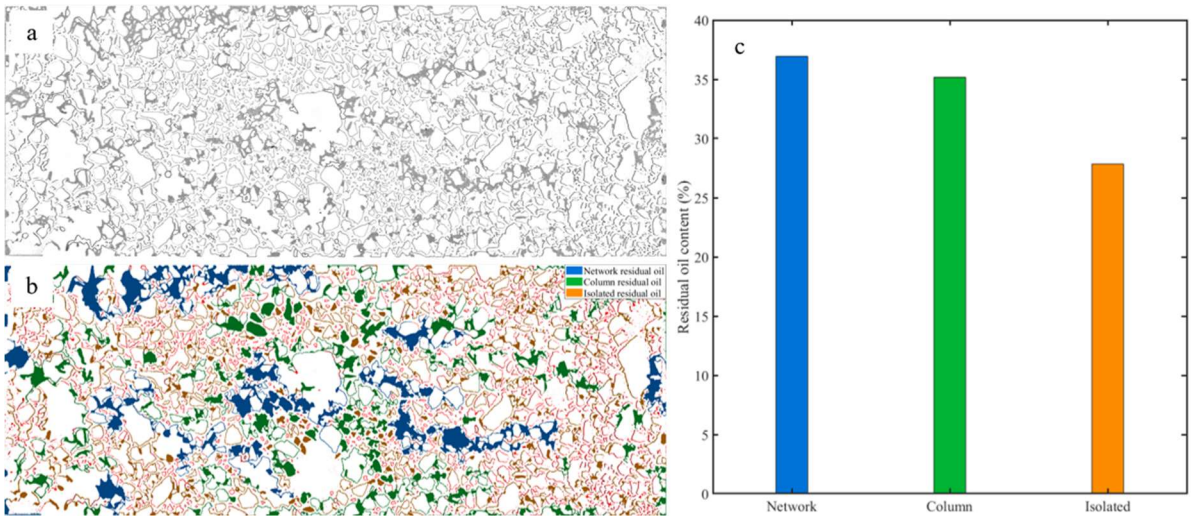

Fig. 7 Residual Oil Storage State in Microfluidic Water Flooding

Quantitative statistical results (Fig c) indicate that the highest proportion of residual oil after waterflooding occurs in the reticular phase (approximately 35%–40%), followed by the columnar phase, while the solitary droplet phase exhibits the lowest residual oil content. This finding demonstrates that, without regulating oil–water interface properties, waterflooding is primarily influenced by pore heterogeneity and unstable advancement, resulting in limitations to both macroscopic sweep efficiency and microscopic displacement efficiency.

3.2. Surfactant Water-Flooding Microfluidic Experiment Results

3.2.1. Surfactant Water-Flood Microfluidic Experiment: Displacement Effect and Interface Evolution Process

Figures (a)–(f) illustrate the temporal evolution of oil phase distribution within the microfluidic chip during surfactant displacement, while Figure (g) presents the corresponding recovery rate curve over time. Compared to conventional water flooding, surfactant displacement demonstrates significantly enhanced micro-scale oil displacement effects. During the initial displacement phase (0–20 s), the surfactant solution rapidly reduces oil–water interfacial tension upon entering the pores. This causes significant deformation and migration of interconnected oil and film-like oil phases, which were previously constrained by capillary forces. Part of the oil phase is stripped and enters the main flow channel, resulting in a rapid increase in recovery rate from 0 to approximately 27%. Microscopic images reveal that the oil phase distribution gradually transitions from a continuous network to irregular clusters. During the intermediate stage (20–60 s), the surfactant continues to act on the oil–water interface. Oil phase at pore throats is further stretched and fractured, significantly reducing connected oil bodies. The remaining oil gradually transforms into smaller-scale isolated oil droplets. Recovery rate steadily increases from approximately 27% to about 38% during this stage, indicating that the surfactant significantly enhances the water phase's ability to mobilize residual oil at the micro-scale. Upon reaching approximately 80 s, displacement enters the intensification stage (80–120 s). Microscopic images reveal numerous isolated oil droplets being mobilized and migrating, with a significant decrease in oil phase area. Recovery rate rapidly increases from about 38% to approximately 63%. This stage primarily reflects the surfactant's displacement contribution, demonstrating the synergistic effects of reduced interfacial tension and improved wettability. During the late displacement phase (120–140 s), residual oil in pores primarily exists as extremely small isolated droplets, making further mobilization increasingly difficult. Recovery growth gradually levels off, ultimately stabilizing at approximately 65%. Overall, surfactant displacement effectively mitigates capillary

ISSN: 2710-0588

entrapment effects and significantly enhances the mobilization of residual oil in tight pores. Its microscopic mechanism primarily involves transforming the oil phase morphology from interconnected to highly dispersed, thereby achieving sustained recovery rate improvement.

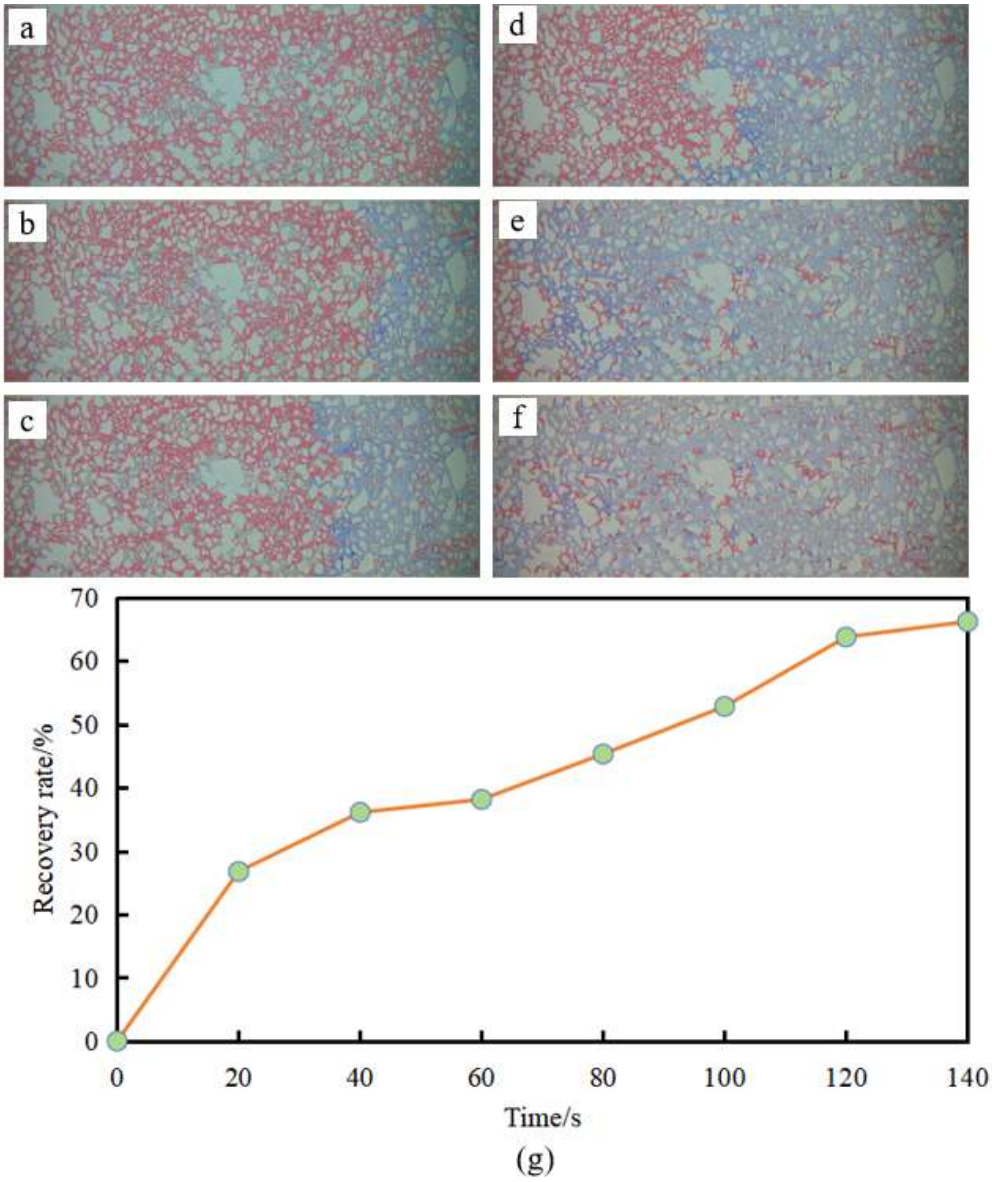

Fig. 8 Microfluidic Surfactant Displacement Results

3.2.2. Microfluidic Experiment on the Micro-Effect of Surfactant Water Flooding

After surfactant addition (Fig. 9(a–c)), the spatial distribution and morphological characteristics of residual oil underwent significant changes. Compared to water flooding, the large-scale continuous network of residual oil in Fig. b markedly decreased, with portions of the original connected oil phase fragmented into smaller columnar or isolated droplet-like residual oil. The addition of surfactants reduced the oil–water interfacial tension and weakened capillary confinement effects, leading to the fracture and redistribution of previously immobile connected oil phases.

ISSN: 2710-0588

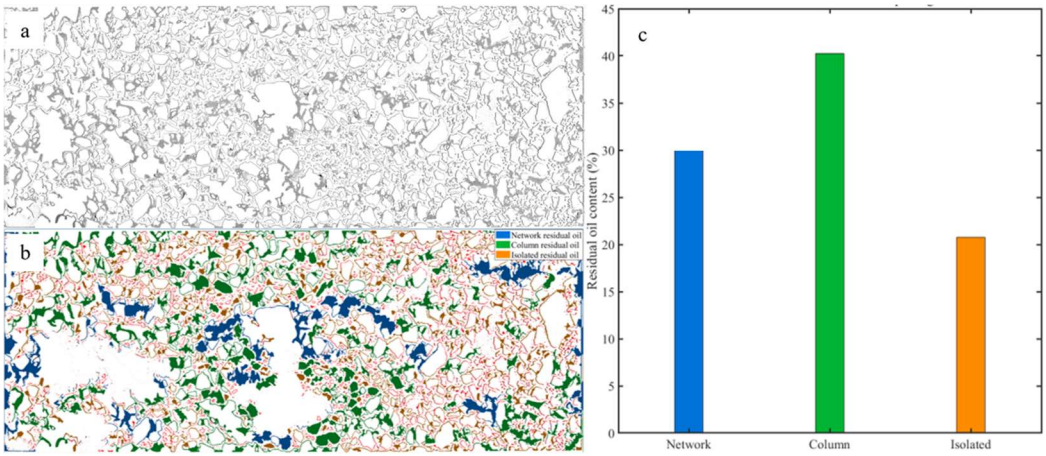

Fig. 9 Residual Oil Storage State in Microfluidic Water Flooding

As shown in the statistical results (Figure c), the proportion of columnar residual oil has increased significantly, while the proportion of isolated droplet residual oil has relatively decreased, and the share of reticular residual oil has further diminished. This indicates that surfactant flooding can effectively disrupt the continuous oil phase structure, converting part of the reticular residual oil into smaller-scale oil phase forms that are more readily displaced by subsequent flooding, thereby improving micro-scale displacement efficiency.

A comparative analysis of the two displacement mechanisms reveals that under waterflooding conditions, residual oil predominantly exists in highly interconnected reticular and columnar structures, reflecting pronounced flow-around effects and limited micro-scale wetting. In contrast, surfactant flooding significantly reduces oil phase connectivity by lowering interfacial tension and improving wetting conditions, thereby promoting the disintegration and restructuring of large-scale residual oil structures.

From a quantitative perspective, surfactants drive the transformation of residual oil morphology from a “predominantly reticular residual oil” state to a “predominantly columnar residual oil” state. This indicates that their primary mechanism of action lies in enhancing pore-scale stripping and reinitiation capabilities, rather than merely expanding macroscopic wave propagation. This morphological transformation provides a more favorable micro-scale foundation for subsequent displacement or composite displacement.

4. Effect of Surfactant Displacement on Residual Oil Storage in Different Pores

As shown in the figure, the distribution characteristics of residual oil in different pore types exhibit significant differences. In macroporosity, residual oil under waterflooding conditions is predominantly columnar oil, followed by network oil, with a relatively low proportion of isolated oil. Surfactant displacement can slightly increase the proportion of network oil. This is primarily attributed to surfactants reducing oil-water interfacial tension and improving pore throat connectivity, thereby mobilizing network-type residual oil that was previously undriven by water. However, columnar oil remains the predominant residual oil type.

In mesopores, columnar oil and isolated droplets dominate under water flooding, with isolated droplets accounting for a significantly higher proportion than in macropores. Surfactant displacement further increases the proportion of free oil while slightly reducing columnar oil, indicating higher stability of free oil in mesopores. Surfactants enhance oil-water interface wettability and reduce capillary confinement forces, thereby mobilizing some columnar oil but having limited effect on free oil.

ISSN: 2710-0588

Within microporosity, residual oil primarily exists as network oil, with relatively low proportions of columnar oil and isolated droplets. This indicates that both water flooding and surfactant displacement struggle to effectively mobilize network oil within microporosity. This phenomenon arises from microporosity's high capillary confinement forces and complex connectivity. While surfactants can reduce interfacial tension, they struggle to significantly alter the mobility state of oil within microporous spaces.

Overall, surfactant displacement demonstrates superior oil recovery efficiency compared to water flooding in both macropores and mesopores. However, isolated oil droplets in mesopores and network oil in micropores remain the predominant residual oil types, indicating that pore type exerts a distinctively selective control over residual oil distribution. This phenomenon reflects the combined mechanism of throat structure, capillary forces, and oil-water interface properties in governing residual oil distribution and recoverability.

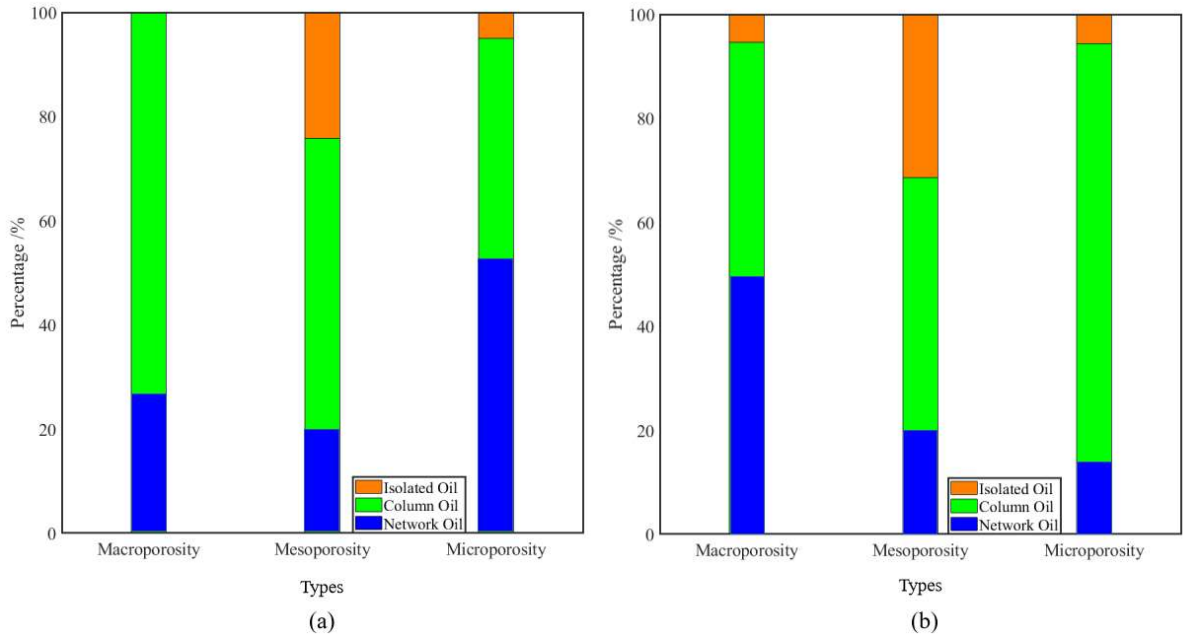

Fig. 10 Comparison of Residual Oil Distribution under Micro-Scale Conditions with Surfactant Treatment

5. Conclusion

This study systematically conducted visualization experiments of surfactant water flooding by constructing a heterogeneous microfluidic chip, thereby revealing the microscopic oil displacement mechanism of surfactants in tight reservoirs. The main conclusions are as follows:

(1) Under conventional waterflooding conditions, the displacement process is governed by dominant flow pathways. Residual oil primarily persists in reticular and columnar forms. Recovery rates increase rapidly before plateauing, ultimately reaching only about 43%. Both micro-saturation efficiency and displacement efficiency remain relatively low.

(2) Surfactant displacement significantly enhanced oil recovery by reducing oil-water interfacial tension and regulating wettability. This process induced deformation, fracture, and redistribution of the oil phase, transforming the residual oil morphology from predominantly interconnected network oil to primarily columnar and isolated droplet oil. Ultimately, the recovery rate increased to approximately 65%, representing a 22 percentage point improvement over water flooding.

ISSN: 2710-0588

(3) Surfactants primarily achieve effective mobilization of residual oil in macropores and mesopores by weakening capillary confinement and enhancing droplet detachment and initiation capabilities. However, in micropores, networked residual oil remains difficult to effectively displace, indicating that pore-scale heterogeneity significantly controls residual oil mobility.

References

[1] Wang Zhe, Cao Guangsheng, Bai Yujie, et al. Current status and prospects of enhanced oil recovery technologies in low permeability reservoirs [J]. Special Oil & Gas Reservoirs, 2023, 30(1): 1-13.

[2] Li L, Zhang D, Su Y, et al. Microfluidic insights into CO_2 sequestration and enhanced oil recovery in laminated shale reservoirs: Post-fracturing interface dynamics and micro-scale mechanisms[J]. Advances in Geo-Energy Research, 2024, 13(3): 203-217.

[3] Yu, Chunlei, Mi Lidong, Wang Chuan, et al. Microscopic percolation characteristics of remaining oil in water-flooded reservoirs at ultra-high water cut stage [J]. Fault-Block Oil & Gas Field, 2016, 23(5): 592-594+598.

[4] Sun Zhe, Wu Xingcai, Kang Xiaodong, et al. Comparison of oil displacement mechanisms and performance between continuous phase and dispersed phase displacement systems [J]. Petroleum Exploration and Development, 2019, 46(1): 116-124.

[5] Medlin W. L, Masse' L, Zumwalt G.L. Method for recovery of oil by means of a gas drive combined with low amplitude seismic excitation [P]. 1983, US Patent US4417621A .

[6] Song Jianping, Chen Jianhua, Liu Bin. Study on enhanced oil recovery technology using low-frequency pulse waves and its field test [J]. Oil Drilling & Production Technology, 1994, (6): 81-87+100.

[7] Zhang Moxi, Chen Xinglong, Lyu Weifeng, et al. Mechanism of microbubble vibration in water-gas dispersion system for enhancing microscopic oil displacement efficiency [J]. Petroleum Exploration and Development, 2024, 51(6): 1363-1373.